IEEE Access
Multidisciplinary | Rapid Review | Open Access Journal

Received March 2, 2021, accepted March 15, 2021, date of publication March 22, 2021, date of current version March 30, 2021.

Digital Object Identifier 10.1109/ACCESS.2021.3067701

Enhancing Distance Protection of Long Transmission Lines Compensated With TCSC and Connected With Wind Power

AHMED ABDEL RAHMAN MOHAMED, HEBATALLAH MOHAMED SHARAF, (Member, IEEE), AND DOAA KHALIL IBRAHIM, (Senior Member, IEEE)

Department of Electrical Power Engineering, Faculty of Engineering, Cairo University, Giza 12613, Egypt

Corresponding author: Hebatallah Mohamed Sharaf (heba_sharaf@eng.cu.edu.eg)

ABSTRACT Thyristor controlled series compensation (TCSC) is widely used in long transmission lines to mainly improve power transfer capability. However, TCSC produces complicated impedance that negatively affects distance protection operation. The wind energy generation system produces additional complexity to the distance protection performance due to the variation of wind speed and fault current level. This paper proposes an integrated scheme to change adaptively the settings of the Mho distance protection by shifting the relay characteristics considering the bad impacts of TCSC, wind power and fault resistance. The proposed scheme achieves its main stages starting from fault detection, until relay tripping decision procedure including online estimation for preliminary fault location, impedance of TCSC and fault resistance using limited communication requirements. By extensive MATLAB simulations, the performance of the proposed scheme is examined compared with the conventional Mho relays under different fault locations, fault inception angle, fault resistance, different wind power penetration, different wind speeds and different TCSC firing angles. The achieved results ensured that the proposed scheme improves significantly Mho distance relay operation and avoids under-reaching and over-reaching problems irrespective of the large shunt capacitance along the transmission line, and also without identifying the parameters of TCSC such as the capacitance, the inductance or the firing angle.

INDEX TERMS Adaptive settings, distance protection, Thyristor controlled series compensation (TCSC), transmission line (TL), wind power.

I. INTRODUCTION

The rapid growth in electrical power demand is a challenge for all energy systems around the world that requires constructing new generation stations and enhancing transmission and distribution facilities. Wind energy is considered one of the best sources of energy because of the environmental concerns. However, the penetration level of wind energy systems in transmission systems has bad impacts on the performance of distance protection [1]. As discussed in [2], [3], wind speed fluctuations cause voltage level variations at local buses so the impedance seen by distance relay will fluctuate affecting significantly the distance relay trip boundaries. For double fed induction generator (DFIG), that is most commonly used for wind energy worldwide, the crowbar resistance causes variation in the fault current which also causes reach concerns in distance protection. Moreover, the combination of rotor winding resistance and the resistance of crowbar will affect the 3-phase faults to be high impedance faults that are considered real challenging for the distance relay to sense [2].

With the increase in transmitted electrical power, Flexible Alternating Current Transmission Systems (FACTS) are applied to improve controlling of network conditions in a fast manner through series and/or shunt compensation. Series compensation devices act as controllable voltage sources to inject voltage in series with the line such as Thyristor controlled series compensation (TCSC). In this type, the series capacitor reduces the line reactance and then increases active power transfer capability [4]. TCSC is one of the most common types of FACTS where it does not require high voltage transformer as interfacing equipment, hence TCSC is more economic than some other FACTS devices [4], [5].

The associate editor coordinating the review of this manuscript and approving it for publication was Arash Asrari.

Also TCSC is confirmed to be robust in alleviating power system operation difficulties such as suppression of the active power oscillations, elimination of sub-synchronous oscillations, and voltage support [4]. Thus, it is firstly chosen worldwide among different FACTS practices [6]. On the other hand, shunt compensation devices, such as static synchronous compensator and static var compensator, perform as controllable current sources by injecting reactive current into the line to maintain voltage magnitude at constant value and improve system power factor and stability. Such functions are achieved by controlling the value of shunt impedance and then increasing transmittable active power but with increasing demand of reactive power [7].

Despite TCSC advantages in increasing power transmission capability, improving system stability, reducing system losses and improving voltage profile of the lines[8], the change in TCSC impedance has great impacts on the impedance measured by distance relay causing mal-operation of conventional distance protection [6], [9]–[14]. For high fault currents, the metal-oxide varistor (MOV) acts and thus then TCSC operates in bypass mode; consequently, the impedance estimated by the distance relay increases which causes relay under-reaching while on the other hand, when the MOV is not activated for high impedance faults, the distance relay estimates an impedance value smaller than the real one, which results in relay over-reaching [11].

Numerous methods have been reported in the literature for applying adaptive settings of distance protection for protecting MOV series compensated transmission lines (TLs). Such methods depend on the impedance calculations of compensator during faults based on the fixed capacitive value and measured fault current flowing through it [15], [16], where the compensator is located at one end as in [15] or both ends as in [16]. Some other research studies have provided distance protection improvement when the compensator is located at the middle of the line as in [17], [18] by calculating the voltage drop across the series compensator depending on the fixed series capacitor. All such methods do not take into consideration the automatic changes of compensation percentage on distance protection and also the impacts of wind farms.

In fact, several research studies have investigated the impacts of TCSC on distance protection but limited studies have provided enhanced distance protection for TCSC compensated lines as in [19]–[21]. For example, the proposed scheme in [19] calculates a dynamic impedance of TCSC during faults depending on the capacitance- inductance impedance where the TCSC is located at one end. In [20], an artificial intelligence based scheme is applied, where the voltage drop across the TCSC, is estimated by using radial basis neural networks, and subtracted it from the voltage measured at distance relays to mitigate the effect of TCSC. Such method is tested for medium length of TLs with fault resistance not more than 20 Ω. The method presented in [21] is tested also for medium length of TLs while the fault resistance was not more than 10 Ω and has considered known parameters of TCSC. Such previously mentioned methods do not consider the penetration of wind energy systems in the protected TLs.

To enhance the distance protection performance for TLs connected to wind energy systems, combining differential and distance protection is proposed in [22]. Such method uses the active power calculations in both ends of the line to calculate the fault resistance and then estimate the fault location. However, it is deduced that its main limitation is ignoring the line resistance with respect to fault resistance, which may not be accepted for long TLs. Improving the coverage of zone 2 of distance relay for TLs connected with double fed induction generator (DFIG) is proposed in [23] and tested for medium length of TLs. It is worth mentioning that both [22] and [23] do not study the impact of such improvements on compensated TLs.

Providing adaptive distance protection settings to protect series compensated TLs connected with wind power is proposed in [24], depending on synchronized voltage and current measurements at both local and remote ends. Besides, the voltage measurements across the compensator and the current through it are also measured to estimate its impedance continuously during fault, which is considered the main drawback. In addition, the impact of ground fault resistance variations on the performance of proposed adaptive distance relay setting is not studied in [24].

Regarding the differential protection as another protection scheme that can be applied for TLs, the weak source of wind farm appears especially after fault inception by few cycles, as discussed in [25], [26], will negatively affect the differential protection performance. In addition, the continuous need to share instantaneous measured data between local and remote relays over long distance is considered another challenge in applying the differential protection for long TLs.

From all of the aforementioned studies, authors believe that there is still much room for developing efficient distance protection schemes for compensated TLs with TCSC and connected to wind energy systems. Therefore, this article presents a proposed distance protection scheme suitable for TCSC compensated TLs connected with wind farms. It will compromise integrated algorithms for distance relay operation starting from fault detection, fault classification and until relay tripping decision procedure. The scheme considers the shunt capacitance along the TL and estimates the fault preliminary location, the impedance of TCSC and the fault resistance without identifying the parameters of the TCSC such as its capacitance, inductance or the firing angle. The proposed distance protection scheme only requires the voltage measurement at the right side of the TCSC beside the local current and voltage measurements of distance relay at each end of the line. Therefore, the proposed method does not need the current and voltage measurement devices at the left side of the TCSC compared with the scheme introduced in [24].

The organization of this paper is presented as follows: the tested long TL system is described in Section II including

the modeling of TCSC and wind farm. The details of the proposed distance protection scheme with its four main stages are fully described in Section III. The communication requirements for implementing the proposed scheme are discussed in Section IV. In Section V, extensive simulation results for evaluating the proposed protection scheme are demonstrated in details. Finally, the conclusions are drawn in Section VI.

II. TESTED LONG TL SYSTEM

The double sources tested TL system is shown in Fig.1-a, it consists of:

- Long TL of 600 km, 345 kV rated voltage and 50 Hz. All the TL parameters are presented in Table 1.
- Source at bus A represents an infinite bus.
- Source at bus B represents a wind farm as presented in Table 2.
- Electrical loads at bus A and bus B, each of 390 MW and 200 Mvar.
- TCSC is located at the middle of the protected TL.

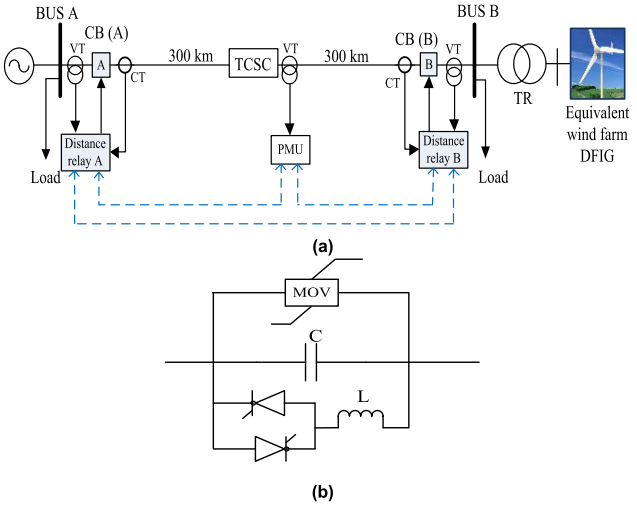

FIGURE 1. Tested TL system. (a) Single line diagram of tested system. (b) TCSC presentation.

TABLE 1. Distributed parameters of the TL [24].

Parameter	Positive sequence	Negative sequence	Zero sequence
R (Ω/km)	0.038806	0.038806	0.1055
L (mH/km)	1.0011	1.0011	1.19599
C (μF/km)	0.01159	0.01159	0.003

A. TCSC MODEL

From a modeling point of view, TCSCs includes continuous elements (inductors and capacitors), as well as discrete elements (power electronic switches). The two main analytical models of TCSC are the quasi-static and the phasor dynamic models [27]. As concluded in [28], a quasi-static model is used in oscillatory stability and transient studies. The reactance of this model is represented at fundamental frequency and its value is based on the value of firing angle so this model is simple but it is not suitable for studies of sub-synchronous resonance where its results are not accurate Hence the phasor dynamic model is suitable for such studies. Phasor dynamic model can be considered as a midway between representation of time-domain circuit and sinusoidal steady-state approximation of quasi-static model, and consequently for improving its accuracy the dynamics of higher order harmonics will be required to take into consideration

For paper work, the TCSC detailed time domain circuit representation in Matlab/Simulink is applied. As discussed in [29], the Matlab TCSC detailed model was improved in simple form and has provide good accuracy with operating conditions and range of system parameters. TCSC is set for the tested TL at 40% line compensation level and presented as illustrated in Fig. 1-b.

TABLE 2. Parameters of wind farm and transformer.

Component	Parameters
Wind farm	150 wind turbines × 1.5 MW, 50 Hz
DFIG of each wind turbine	Rotor resistance = 0.016 p.u, Rotor inductance = 0.16 p.u Stator resistance =0.023 p.u, Stator inductance = 0.18 p.u Magnetizing inductance = 2.9 p.u, Inertia constant = 0.685 s, Friction factor = 0.01 p.u Pairs of poles = 3
Transformer	575 V/345 kV, 150 × 2 MVA

B. WIND FARM MODEL

The wind farm, located at bus B, consists of 150 turbines × 1.5 MW based on DFIG. The detailed parameters of DFIG of each wind turbine are set according to MATLAB/Simulink library [30], as presented in Table 2.

The stator of DFIG is directly connected to the grid, while its rotor is connected to the grid via a bi-directional voltage source converter (VSC) to achieve good dynamic performance [31]. The detailed model available in Matlab Specialized Power Systems: Renewable Energy Systems to accurately model VSC based energy conversion systems connected to power grids [30] is applied for paper work. It includes detailed representation of power electronics for IGBT (insulated-gate bipolar transistor) converters to achieve an acceptable accuracy with switching frequencies. The model is discretized at 5 microseconds as a small time step to be suited for observing control system dynamic performance over relatively short periods of times. The steady-state and dynamic performance of the model is investigated to approve its robustness when observing the turbine response to wind speed changes, and the impact of voltage sag resulting from remote faults.

III. PROPOSED MHO DISTANCE PROTECTION SCHEME

For the generalization of the proposed scheme to be suitable for any TL compensated with TCSC and connected to wind

power, four main stages are implemented starting from fault detection, until relay tripping decision procedure as follows:

- 1st stage: fault detection and distinguishing faults behind or in front of TCSC.
- 2nd stage: fault types classification.
- 3rd stage: calculating online fault location, TCSC impedance and fault resistance.
- 4th stage: adaptive settings of Mho distance relay.

A. THE FIRST STAGE: FAULT DETECTION

In this stage, any fault event is detected and its position with respect to TCSC (in front of it or behind it) is also distinguished. At first, only one-level discrete wavelet decomposition is applied with the fourth order Daubechies (db4) as a mother wavelet for the Clark transformed voltage signals at relays A and B with 200 kHz sampling frequency to capture sufficient fault transient information. To extract the transient traveling waves mainly between 50 and 100 kHz, the absolute sum for first detail ($d1$) of both zero (0) and beta (β) modes are captured for 1 cycle moving window (sample by sample) until fault detection. The mathematical formulation in Eqn. (1) is used to calculate the absolute sum at k sample, where n presents a sample order in a sliding window covering a complete power cycle (20 ms), and N is the total number of samples in a cycle.

$$\left.\begin{aligned} Sum_0(k) &= \sum_{n=k-N+1}^{k} |d1\_V_0(n)| \\ Sum_\beta(k) &= \sum_{n=k-N+1}^{k} |d1\_V_\beta(n)| \end{aligned}\right\} \quad (1)$$

At the instant of fault detection, Sum_0, Sum_β or both exceed the threshold values th_0 and th_β (which denote zero and beta mode threshold respectively). Besides, when Sum_0 exceeds the threshold th_0, a fault is discriminated as a ground fault.

In fact, this implemented algorithm is similar to the procedure discussed in several reported studies such as in [32] but with Clark mode signals instead of phase signals. It is noteworthy that the threshold values were determined by extensively testing the studied system in several normal and faulted cases.

After the fault is detected, it will be distinguished either behind or in front of TCSC by comparing the fault detection time for both relays A and B (t_A and t_B respectively). The time-synchronization is required to provide the reference time for comparing the two estimated times. As described in Fig. 1-a, the TCSC is located at the middle of protected TL, so if t_A is more than t_B, the fault is distinguished to be between the TCSC and bus B (in front of TCSC), otherwise it is distinguished to be behind the TCSC (between bus A and TCSC). Fig. 2 summarizes the flowchart for the fault detection.

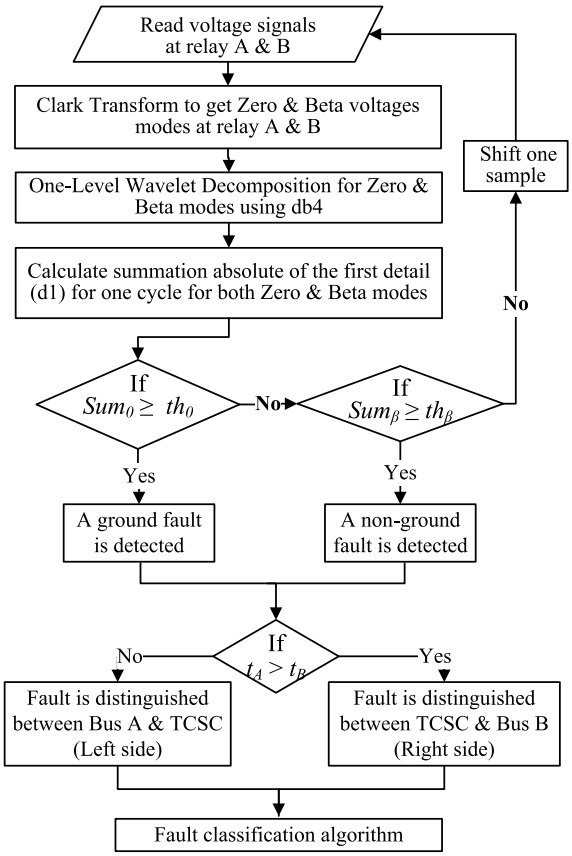

FIGURE 2. Flowchart for the fault detection algorithm.

As an example, phase A to ground (AG) fault occurs at 400 km at 0.5 s fault inception time with 100 Ω fault resistance, Fig. 3-a illustrates the measured voltage signals at relays A and B. By implementing the fault detection algorithm, Fig. 3-b compares t_A and t_B, as revealed, relay A has detected such fault at $t_A = 0.5004$ s while relay B has detected it earlier at 0.5001 s, which ensures that the fault is between TCSC and relay B.

B. THE SECOND STAGE: FAULT CLASSIFICATION

This section explains the applied algorithm for fault type classification by comparing root mean square (RMS) values calculated by using discrete Fourier transform (DFT) for local voltages and currents at relays A and B before and after the fault inception. It simply depends on the fact that the voltage of faulty phase(s) decreases, whereas the current of the faulty phase(s) rises significantly [33]. So, the applied algorithm reduces the computational burden as it does not depend on any threshold values as shown in the flowchart of Fig. 4, where V_{a2}, V_{b2} and V_{c2} describe the 3-ph RMS voltages after the fault inception compared with corresponding values before the fault (V_{a1}, V_{b1} and V_{c1}), with similar notations for currents.

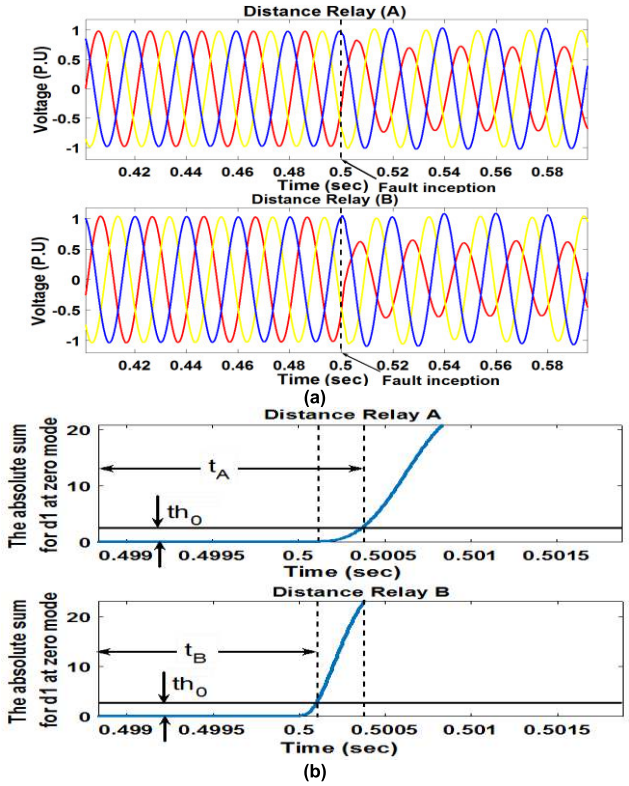

FIGURE 3. A-G fault occurs at 400 km, 100 Ω fault resistance at 0.5 s fault inception time. (a) Voltage signals (b) The absolute sum for first detail coefficients (d1) signals.

C. THE THIRD STAGE: ONLINE FAULT LOCATION ESTIMATION

A fault location algorithm, based on the transmission line ABCD parameters and phase sequences, is presented in [34] for TL with MOV series compensator but without considering the impact of connecting wind energy systems to the TL. Such method is modified here to be applied for TCSC compensated TL connected with wind farms.

To describe the applied methodology, a fault is simulated behind the TCSC as shown in Fig. 5 at $x = L_f$. The developed algorithm is based on online fault location calculation by using ABCD parameters of the TL. At first, DFT is applied to calculate RMS values for phase voltages and currents at 1.25 cycles after the instant of fault detection. The algorithm requires the calculated RMS values for 3-phase voltage and current at TL ends (at relay A and B) and for 3-phase voltage after TCSC. These RMS values are converted using Clarke transformation to zero, alpha and beta (0–α–β) [35]. The ABCD parameter equations, based on Clarke components, are used to calculate voltages, $V_{x(m)}$, and fault currents coming from bus A, $I_{xA(m)}$, along the transmission line by changing distance, x, from 1 km until the TCSC location (at 300 km) by incrementing 1 km step as shown in Eqn. (2) where, m, refers to modes 0–α–β components. Eqns. (3)-(4) are used to calculate the currents pass through TCSC as function of x. Eqn. (5) is used to calculate the fault current coming from bus B as function of x.

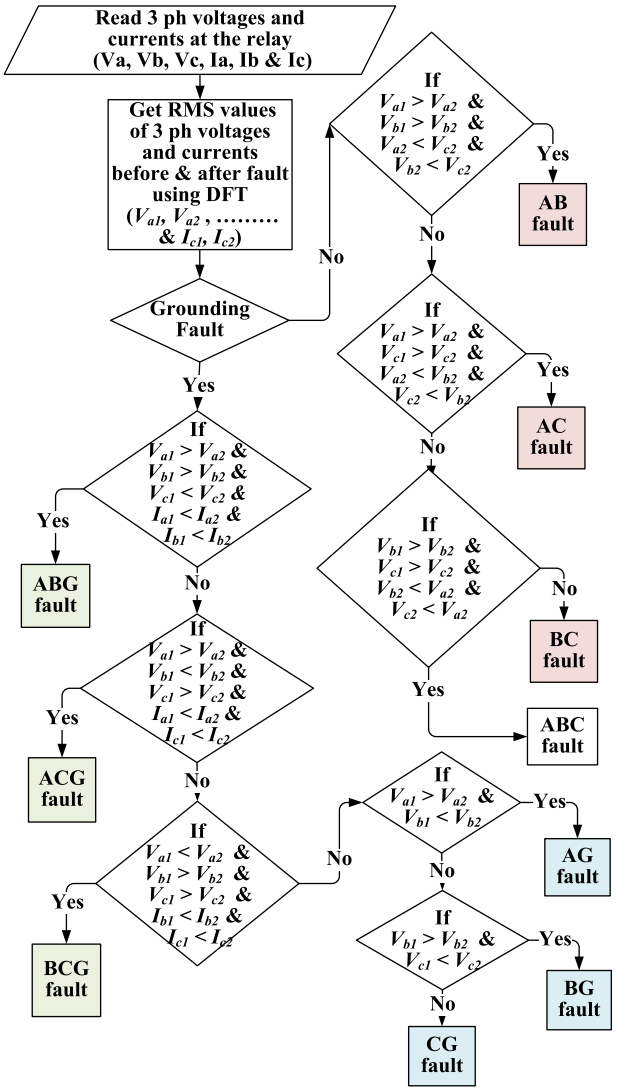

FIGURE 4. Flowchart for the fault classification algorithm.

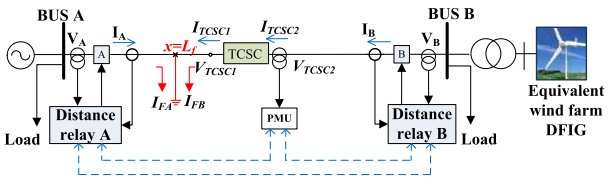

FIGURE 5. A fault is simulated behind TCSC (between bus A and TCSC) at $x = L_f$.

Then, the inverse Clark transform is applied to convert the calculated 0–α–β components for voltages and currents to 3-phase voltages and currents and subsequently the voltages and currents of faulty phase(s) will be considered. As shown in Eqn. (6), the faulty phase(s) currents I_{xA} and I_{xB} are the inverse Clark transformation of $I_{xA(m)}$ and $I_{xB(m)}$ respectively.

Consequently, the minimum difference angle between V_x and I_x along the faulty phase (θ_x) will be captured to indicate the estimated fault location (L_{f_est}) [34]. Besides, this method

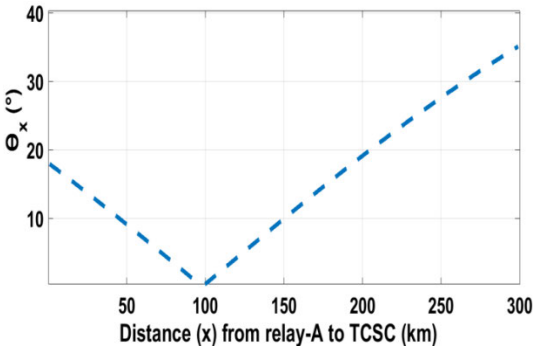

FIGURE 6. Online fault location estimation at L_{f_est} = 99 km for a fault exists behind TCSC at 100 km from relay A.

calculates the voltage at left side of TCSC, $V_{TCSC1(m)}$, in *0*-α-β components as expressed in Eqn. (7) so the impedance of TCSC, Z_{TCSC}, and fault resistance, R_F, can be estimated as shown in Eqns. (8) and (9).

$$\begin{pmatrix} V_{x(m)} \\ -I_{xA(m)} \end{pmatrix} = \begin{bmatrix} A_{x(m)} & B_{x(m)} \\ C_{x(m)} & D_{x(m)} \end{bmatrix} \begin{pmatrix} V_{A(m)} \\ -I_{A(m)} \end{pmatrix} \quad (2)$$

$$I_{TCSC2(xm)} = -C_{x(m)}V_{B(m)} + D_{x(m)}I_{B(m)} \quad (3)$$

$$I_{TCSC1(xm)} = I_{TCSC2(xm)} \quad (4)$$

$$I_{xB(m)} = \frac{(I_{TSCS1(xm)}(C_{x(m)}V_{x(m)}))}{D_x} \quad (5)$$

$$I_x = I_{xA} + I_{xB} \quad (6)$$

$$V_{TCSC1(m)} = A_{F(m)}V_{F(m)} - B_{F(m)}I_{FB(m)} \quad (7)$$

$$Z_{TCSC} = \frac{(V_{TSCS2} - V_{TCSC1})}{I_{TCSC2}} \quad (8)$$

$$R_F = \frac{V_F}{I_F} \quad (9)$$

where:

- $V_{A(m)}$ an $I_{A(m)}$ ddescribe *0*-α-β voltages and currents at bus A,
- $V_{B(m)}$ an $I_{B(m)}$ d describe *0*-α-β voltages and currents at bus B,
- V_x an I_x ddescribe the calculated faulty phase voltage and current as function of x,
- V_{TCSC2} is the phase voltages at right side of TCSC,
- V_F and I_F are the calculated phase voltages and currents at fault location,
- R_F is the estimated fault resistance.

As an example, consider AG fault occurs behind TCSC at 100 km from relay A with 0° inception angle, 100 Ω fault resistance and 15 m/s wind speed. For such fault, the algorithm has located it at 99 km from relay A (L_{f_est}), as proved in Fig. 6 at the minimum difference angle between V_x and I_x (θ_x).

It must be pointed out that, Eqn. (9) estimates the fault resistance for SLG fault, while for double line to line fault (e.g. BC fault), V_F and I_F will be the difference between the faulty phases voltage and currents respectively [36].

As a matter of fact, ABCD parameters for long TL at any distance x can be calculated by Eqns. (10) where Z_C and γ denote the characteristic impedance and propagation constant, respectively [37]:

$$\begin{cases} A_{x(m)} = D_{x(m)} = cosh\gamma_{(m)}x \\ B_{x(m)} = Z_{C(m)}Sinh\gamma_{(m)}x \\ C_{x(m)} = \dfrac{Sinh\gamma_{(m)}x}{Z_{C(m)}} \end{cases} \quad (10)$$

Same procedure and modified equations are applied for faults exist in front of TCSC (between bus B and TCSC).

The flowchart that describes how the methodology of online fault location calculation is implemented as demonstrated in Fig. 7.

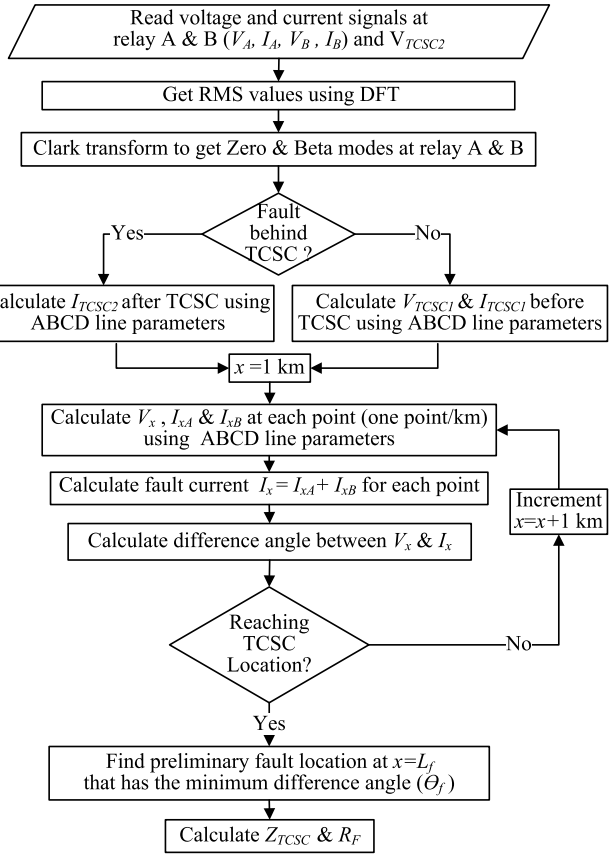

FIGURE 7. Flowchart for online fault location estimation.

D. THE FOURTH STAGE: ADAPTIVE SETTINGS OF MHO DISTANCE RELAY

As known, Mho relay is the most popular distance relay used, as Mho relay has economical and easy comparator implementation feature. The conventional Mho distance relay takes the local phase currents and voltages continuously and then their magnitudes and phase angles are calculated using DFT to calculate the apparent impedance trajectory as illustrated in Table 3 for different fault types where Z_{L1},Z_{L0} present the positive and zero sequence line impedance respectively, while I_0 describes the zero sequence current.

TABLE 3. Apparent impedance seen by distance relay [36].

Fault Type	Calculated Impedance
AG	$V_a/(I_a + 3K_0.I_0)$ where $K_0 = \frac{Z_{L0}-Z_{L1}}{3Z_{L1}}$
ABG or AB	$(V_a - V_b)/(I_a - I_b)$
ABC	(V_a/I_a) *or* (V_b/I_b) *or* (V_c/I_c)

Typically, the first zone setting (L_{set1}) and the secondzone (L_{set2}) of Mho distance are taken at 80% and 120% of the protected TL length respectively. Accordingly, during faults the apparent impedance trajectory will be inside its zones to detect the fault in its corresponding zone and issue a correct trip at the required time. But, as discussed before, the conventional distance relay fails to determine the correct fault zone due to the effects of TCSC, wind farm and also the fault resistance.

To overcome such mal-operation, a proposed procedure for adaptive settings of Mho distance relay is implemented here in the fourth stage of the proposed relay as will be shown in the flowchart of Fig. 8 for Relay A.

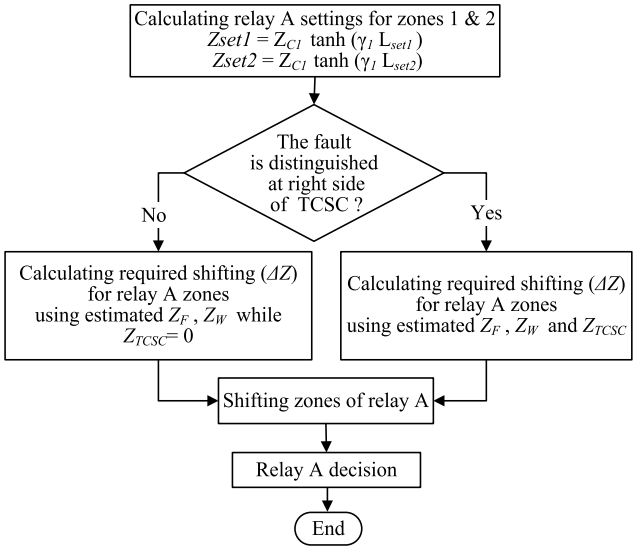

FIGURE 8. Flowchart for Mho distance relay adaptive setting.

It is based on applying a shifting (ΔZ) for its zones circles using the calculated TCSC impedance (Z_{TCSC}), calculated fault impedance (Z_F) and also (Z_w) that represents the mitigation for wind farm effects as follows:

$$Z_w = Z_{relay} - \left(Z_F + Z_{TCSC} + \left(Z_{C1} tanh\left(\gamma_1 L_{f\_est}\right)\right)\right) \quad (11)$$

$$where: Z_{C1} = \sqrt{\frac{Z_{T1}}{Y_{T1}}}, \gamma_1 = \sqrt{Z_{T1}Y_{T1}}$$

$$\Delta Z = Z_F + Z_{TCSC} + Z_w \quad (12)$$

where:

- Z_F: Fault impedance seen by distance relay depending on the calculated fault resistance R_F (in 3rd stage) and fault type (classified in 2nd stage).
- Z_{relay}: Impedance seen by distance relay at 1.25 cycles after the fault is detected (in 1st stage).
- Z_{TCSC}: Calculated impedance of TCSC (in 3rd stage).
- L_{f_est}: Estimated online fault location (in 3rd stage).
- Z_{C1}, γ_1: TL Positive sequence characteristic impedance and propagation constant, respectively.
- Z_{T1}, Y_{T1}: TL Positive sequence impedance and admittance, respectively.

E. DETAILED EXAMPLE FOR THE IMPLEMENTATION OF THE PROPOSED MHO DISTANCE RELAY

Assuming an AG fault occurs nearly to the boundary of the first zone of relay A at 465 km (77.5 % of the protected TL). Such fault is simulated at 0.505 s, and 200 Ω fault resistance. The proposed Mho distance relay is implemented as follows:

- ➢ By applying the 1st stage algorithm, the fault is detected by relay A and B at 0.5054 and 0.5051 s respectively and thus the fault is discriminated in front of the TCSC.
- ➢ Consequently, the fault is classified accurately in 2nd stage.
- ➢ By applying the 3rd stage, R_F is estimated by 200.3762 Ω, while the TCSC impedance is estimated by $81.4165\Omega\angle -85.3811°$ and the fault location is estimated at 468 km.
- ➢ By applying the 4th stage, the fault impedance seen by distance relay A (Z_F) is estimated by $230.6791\Omega\angle -15.1517^{\circ}$ using the formula:

$$Z_F = \frac{I_F.R_F}{I_a + 3K_0.I_0}, \quad \text{where } K_0 = \frac{Z_{L0} - Z_{L1}}{3Z_{L1}} \quad (13)$$

where: K_0 is the zero-sequence current compensation factor, Z_{L1}, Z_{L0} are the positive and zero sequence TL impedance respectively, while I_0 describes the zero sequence current.

- ➢ Accordingly, the shift required for the zones characteristics (ΔZ) is estimated by $\Delta Z = 278.1069\Omega\angle -28.6826°$ and then the tripping characteristics are adaptively shifted.

As shown in Fig. 9, the conventional relay has failed in detecting such fault as the impedance seen by the relay was out of its zones. On the other hand, the proposed scheme,

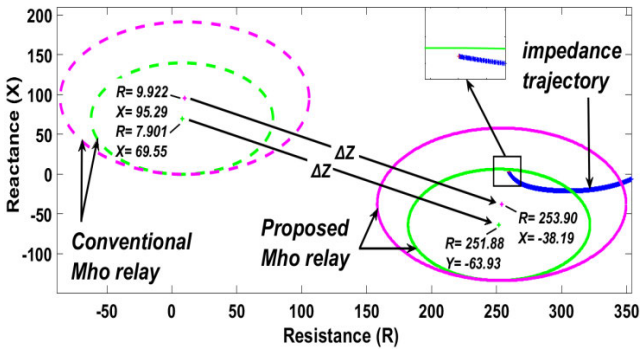

FIGURE 9. Performance of proposed Mho relay versus the conventional one during AG fault at 465 km and 200 Ω fault resistance.

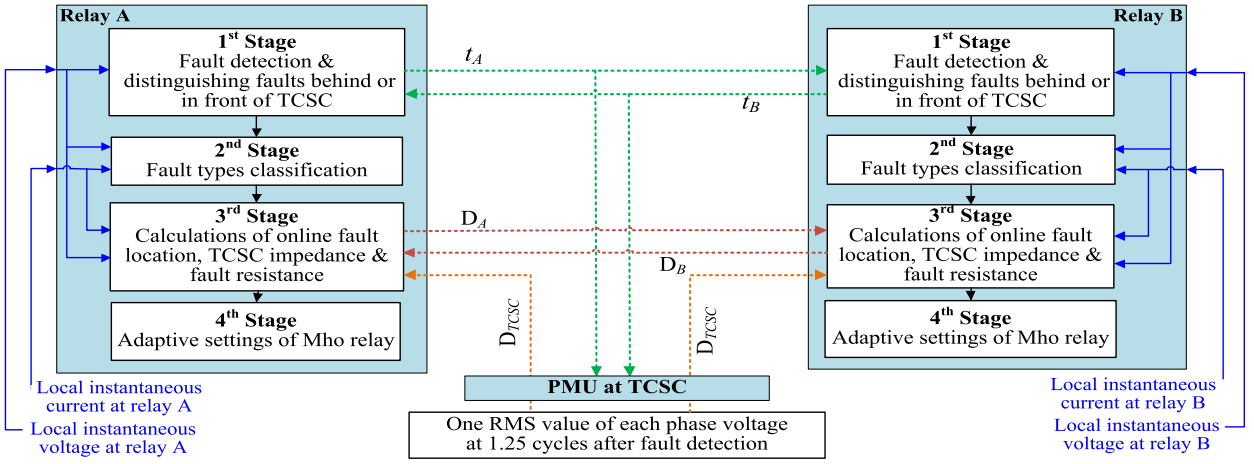

FIGURE 10. Block diagram for implementing the proposed scheme for relay A and B (at the two end of the protected TL).

by applying this shifting for its Mho characteristics, has succeeded in detecting the fault accurately in the first zone and thus the negative impacts of fault impedance, TCSC impedance and wind farm are mitigated.

IV. COMMUNICATION REQUIREMENTS FOR IMPLEMENTING PROPOSED SCHEME

To ensure the applicability of the proposed scheme, the communication requirements are discussed here for all implemented stages as illustrated in Fig. 10.

During the 1st stage, each distance relay, A or B, detects the fault using its local voltage measurements. Then, each relay sends the detection time to the other relay to distinguish whether the fault is behind or in front of TCSC by comparing the fault detection times at both relay (t_A and t_B). For achieving such comparison, same reference time is required for these two estimated times. In addition, each relay will send its detection time to the phasor management unit (PMU) located at TCSC. In the subsequent stages, both distance relays and PMU will use the smallest fault detection time either t_A or t_B.

In the 2nd stage, each relay, A or B, will classify the fault type using its local current and voltage measurements without any transferred data.

In the 3rd stage, each relay will send to the other relay one calculated RMS value per phase for the measured voltage and current at the instant of 1.25 cycles after fault detection. PMU also will send one RMS value per phase for the measured voltage after TCSC to both relays at instant 1.25 cycles after fault detection.

In the 4th stage, each relay operates locally to update its zones adaptively.

Therefore, it can be concluded that the communication requirements for implementing the proposed relay are simple; as one time value is transferred in the 1st stage, while limited RMS values, not instantaneous values, are transferred in the 3rd stage.

V. PERFORMANCE EVALUATION

To ensure the accuracy and effectiveness of the proposed scheme, it is extensively tested under different case studies including different fault locations, fault resistance, fault inception angle as displayed in Table 4. The proposed scheme is tested also at different wind power penetration, different wind speeds as revealed in Tables 5 and 6 and different firing angles of TCSC as displayed in Table 7.In all of the following result tables, some symbols are used as follows:

- "U" indicates under-reach problem where zone 1 is the correct zone while the relay detects it at zone 2.
- "U*" indicates under-reach problem where zone 1 or 2 is the correct zone while the relay detects it out of both zones 1 or 2,
- "O" indicates over-reach problem where zone 2 is the correct zone while the relay detects it at zone 1, an
- "CZ1" and "CZ2" indicate that the correct zone is 1 and 2 respectively.

A. EFFECT OF FAULT CONDITIONS

In this subsection, the proposed scheme at relay A and B has been tested at different fault locations (along the whole TL), different fault inception angles (0°, 45°, and 90°) and different fault resistance values (0, 10, 20, 100, and 200 Ω). The testes are carried out with the assumption of 15 m/s wind speed and 150 × 1.5 MW connected wind farm. The tested faults cover different fault types including A-G fault as a single line A-to-ground fault, BC-G (phase B to C to ground) as a double line to ground fault, BC fault as a line-to- line fault and 3 phase fault.

The proposed scheme performance has been extensively examined in Table 4 compared with respect to the conven-

TABLE 4. The performance of the proposed distance protection scheme compared with the conventional relay in different fault conditions.

For SLG faults									
Actual fault conditions				Conventional distance relay		Proposed scheme			
						Instant of fault detection		Tripping zone	
Fault location (km)	Fault resistance (Ω)	Fault inception (°)	Instant of fault	Relay A	Relay B	Relay A	Relay B	Relay A	Relay B
2	0	0	0.500	CZ1	U*	0.500015	0.5007		
25	100	45	0.505	U*	U*	0.50502	0.5054		CZ2
50	200	0	0.500	U*	U*	0.5001	0.5008		
75	0	45	0.505	CZ1	U*	0.505015	0.5053		
100	100	90	0.510	U*	U*	0.5101	0.5106		
125	200	0	0.500	U*	U*	0.5001	0.5006		
150	0	90	0.510	CZ1	U*	0.510045	0.5104		
175	100	0	0.500	U*	U*	0.5001	0.5005		
200	200	45	0.505	U*	U*	0.5051	0.5053		
225	0	90	0.510	CZ1	U*	0.5101	0.5103	CZ1	
250	100	0	0.500	U*	U*	0.5002	0.5004		
275	200	90	0.510	U*	U*	0.5102	0.5103		
301	200	90	0.510	U*	U*	0.5103	0.510295		
325	0	0	0.500	U	U*	0.5003	0.5001		
350	100	90	0.510	U*	U*	0.5104	0.5102		CZ1
375	200	0	0.500	U*	U*	0.5005	0.5002		
400	0	90	0.510	CZ1	U*	0.5104	0.5101		
425	100	0	0.500	U*	U*	0.5005	0.5001		
450	200	0	0.500	U*	U*	0.5006	0.5001		
475	0	45	0.505	CZ1	U*	0.5053	0.50502		
500	100	45	0.505	U*	U*	0.5054	0.50505		
525	200	90	0.510	U*	U*	0.5107	0.5101		
550	0	45	0.505	O	U*	0.5053	0.505015	CZ2	
575	100	90	0.510	U*	U*	0.5107	0.510025		
598	200	0	0.500	U*	U*	0.5009	0.500015		

For ABC faults									
Actual fault conditions				Conventional distance relay		Proposed scheme			
						Instant of fault detection		Tripping zone	
Fault location (km)	Fault resistance (Ω)	Fault inception (°)	Instant of fault	Relay A	Relay B	Relay A	Relay B	Relay A	Relay B
2	1	0	0.500	CZ1	U*	0.500015	0.5018		
25	10	45	0.505	CZ1	U*	0.5055	0.5090		
50	20	0	0.500	CZ1	U*	0.5002	0.5017		CZ2
75	1	45	0.505	CZ1	U*	0.5062	0.5086		
100	10	90	0.510	CZ1	U*	0.5103	0.5115		
125	20	45	0.505	CZ1	U*	0.5068	0.5084		
150	1	90	0.510	CZ1	U*	0.5104	0.5113		
175	10	0	0.500	CZ1	U*	0.5004	0.5013		
200	20	45	0.505	CZ1	U*	0.5075	0.5078		
225	1	90	0.510	CZ1	U*	0.5105	0.5110	CZ1	
250	10	0	0.500	CZ1	U*	0.5007	0.5010		
275	20	90	0.510	CZ1	U*	0.51078	0.510815		
301	20	90	0.510	U*	U*	0.5109	0.5107		
325	1	0	0.500	U*	U*	0.5008	0.5006		
350	10	90	0.510	U*	U*	0.5110	0.5106		CZ1
375	20	0	0.500	U*	U*	0.5012	0.5006		
400	1	90	0.510	CZ1	U*	0.5112	0.5104		
425	10	0	0.500	CZ1	U*	0.5014	0.5004		
450	20	0	0.500	U	U*	0.5015	0.5004		
475	1	45	0.505	CZ1	U*	0.5084	0.5065		
500	10	45	0.505	O	U*	0.5089	0.5063		
525	20	90	0.510	CZ2	U*	0.5119	0.5102		
550	1	45	0.505	O	U*	0.5091	0.5059	CZ2	
575	10	90	0.510	O	U*	0.5121	0.5101		
598	20	0	0.500	CZ2	U*	0.5025	0.500015		

For BC-G faults									
Actual fault conditions				Conventional distance relay		Proposed scheme			
						Instant of fault detection		Tripping zone	
Fault location (km)	Fault resistance (Ω)	Fault inception (°)	Instant of fault	Relay A	Relay B	Relay A	Relay B	Relay A	Relay B
2	0	0	0.500	CZ1	U*	0.500015	0.5008		
25	100	45	0.505	CZ1	U*	0.50502	0.5055		CZ2
50	200	0	0.500	CZ1	U*	0.5001	0.5013		
75	0	45	0.505	CZ1	U*	0.505015	0.5054		
100	100	90	0.510	CZ1	U*	0.5101	0.5107		
125	200	0	0.500	CZ1	U*	0.5002	0.5008		
150	0	90	0.510	CZ1	U*	0.5101	0.5105		
175	100	0	0.500	CZ1	U*	0.5002	0.5006		
200	200	45	0.505	CZ1	U*	0.5051	0.5054		
225	0	90	0.510	CZ1	U*	0.5101	0.5104	CZ1	
250	100	0	0.500	CZ1	U*	0.5002	0.5004		
275	200	90	0.510	CZ1	U*	0.5103	0.5104		
301	200	90	0.510	CZ1	U*	0.5104	0.5101		
325	0	0	0.500	CZ1	U*	0.5003	0.5001		
350	100	90	0.510	CZ1	U*	0.5104	0.5102		CZ1
375	200	0	0.500	CZ1	U*	0.5006	0.5003		
400	0	90	0.510	CZ1	U*	0.5104	0.5101		
425	100	0	0.500	CZ1	U*	0.5006	0.5002		
450	200	0	0.500	CZ1	U*	0.5006	0.5002		
475	0	90	0.510	CZ1	U*	0.5105	0.51004		
500	100	45	0.505	O	U*	0.5054	0.5051		
525	200	90	0.510	O	U*	0.5108	0.5101		
550	0	45	0.505	O	U*	0.5054	0.505015	CZ2	
575	100	90	0.510	O	U*	0.5108	0.510035		
598	200	0	0.500	O	U*	0.5011	0.500015		

For BC faults									
Actual fault conditions				Conventional distance relay		Proposed scheme			
						Instant of fault detection		Tripping zone	
Fault location (km)	Fault resistance (Ω)	Fault inception (°)	Instant of fault	Relay A	Relay B	Relay A	Relay B	Relay A	Relay B
2	1	0	0.500	CZ1	CZ2	0.500015	0.5018		
25	10	45	0.505	CZ1	U*	0.5055	0.5087		CZ2
50	20	0	0.500	CZ1	U*	0.5002	0.5017		
75	1	45	0.505	CZ1	U*	0.5062	0.5083		
100	10	90	0.510	CZ1	U*	0.5103	0.5115		
125	20	0	0.500	CZ1	U	0.5003	0.5015		
150	1	90	0.510	CZ1	U*	0.5104	0.5113		
175	10	0	0.500	CZ1	U*	0.5004	0.5013		
200	20	45	0.505	CZ1	U*	0.5075	0.5077		
225	1	90	0.510	CZ1	U*	0.5105	0.5110	CZ1	
250	10	0	0.500	CZ1	U*	0.5007	0.5010		
275	20	90	0.510	CZ1	U*	0.51078	0.510815		
301	20	90	0.510	U*	U*	0.5109	0.5107		
325	1	0	0.500	CZ1	U*	0.5008	0.5006		
350	10	90	0.510	CZ1	U*	0.5112	0.5104		CZ1
375	20	0	0.500	CZ1	U*	0.5012	0.5006		
400	1	90	0.510	CZ1	U*	0.5112	0.5104		
425	10	0	0.500	CZ1	U*	0.5014	0.5004		
450	20	0	0.500	U	U*	0.5015	0.5004		
475	1	90	0.510	CZ1	U*	0.5115	0.5103		
500	10	45	0.505	O	U*	0.5089	0.5063		
525	20	90	0.510	O	U*	0.5119	0.5102		
550	1	45	0.505	O	U*	0.5091	0.5059	CZ2	
575	10	90	0.510	O	U*	0.5121	0.5101		
598	20	0	0.500	CZ2	U*	0.5025	0.500015		

tional relay performance. As shown, the conventional Mho distance relay failed to detect faults in its true zones where the under-reach and over-reach problems appear in numerous fault cases especially the relay B at the wind farm side. On the other hand, the proposed scheme has successfully improved the operation of A and B distance relays by avoiding under-reach and over-reach problems at different fault resistance, different fault inception angle and different fault types as well. It is also ensured that the fault detection takes not more than 4.1 ms after fault inception.

TABLE 5. The performance of the proposed distance protection scheme compared with the conventional relay at 15 m/s wind speed for different wind power penetration level.

For SLG faults at 100 Ω fault resistance and 0° fault inception angle						For ABC faults at 20 Ω fault resistance and 0° fault inception angle					
Fault location and wind power conditions		Conventional distance relay		Tripping zone of proposed scheme		Fault location and wind power conditions		Conventional distance relay		Tripping zone of proposed scheme	
Fault location (km)	Wind power (MW)	Relay A	Relay B	Relay A	Relay B	Fault location (km)	Wind power (MW)	Relay A	Relay B	Relay A	Relay B
2	50 × 1.5	U*	U*	CZ1	CZ2	2	50 × 1.5	U	U*	CZ1	CZ2
100	100 × 1.5	U*	U*			100	100 × 1.5	CZ1	U*		
200	150 × 1.5	U*	U*		CZ1	200	150 × 1.5	CZ1	U*		CZ1
301	200 × 1.5	U*	U*			301	200 × 1.5	U*	U*		
400	50 × 1.5	U*	U*			400	50 × 1.5	U	U*		
500	100 × 1.5	U*	U*	CZ2		500	100 × 1.5	CZ2	U*	CZ2	
598	150 × 1.5	U*	U*			598	150 × 1.5	U*	U*		
For BC-G faults at 100 Ω fault resistance and 0° fault inception angle						For BC faults at 20 Ω fault resistance and 0° fault inception angle					
Fault location and wind power conditions		Conventional distance relay		Tripping zone of proposed scheme		Fault location and wind power conditions		Conventional distance relay		Tripping zone of proposed scheme	
Fault location (km)	Wind power (MW)	Relay A	Relay B	Relay A	Relay B	Fault location (km)	Wind power (MW)	Relay A	Relay B	Relay A	Relay B
2	50 × 1.5	CZ1	U*	CZ1	CZ2	2	50 × 1.5	U	U*	CZ1	CZ2
100	100 × 1.5	CZ1	U*			100	100 × 1.5	CZ1	U*		
200	150 × 1.5	CZ1	U*		CZ1	200	150 × 1.5	CZ1	U*		CZ1
301	200 × 1.5	CZ1	U*			301	200 × 1.5	U*	U*		
400	50 × 1.5	CZ1	U*			400	50 × 1.5	CZ1	U*		
500	100 × 1.5	O	U*	CZ2		500	100 × 1.5	O	U*	CZ2	
598	150 × 1.5	O	U*			598	150 × 1.5	CZ2	U*		

Regarding the performance for some faults occurring at critical locations, either near zone boundaries or near buses, for example:

- The conventional Mho distance relay failed to detect faults occurred near to the beginning of the second zone of relay A at 500 km (83.3 % of the protected TL) for different fault resistance (10 and 100Ω) while the proposed scheme has succeeded in detecting the fault accurately at its true protection zone (proposed relays A and B detected such faults at zone 2 and 1 respectively).
- It also can be noticed that the proposed scheme has succeeded to detect the faults very near to buses A and B (at 2 and 598 km respectively) at the correct protection zones.

Therefore, it can be concluded that the proposed scheme is suitable for long TLs and does not depend on known TCSC parameters such as the capacitance, the inductance or the firing angle. It has also ensured its effectiveness at high fault resistance up to 200 Ω compared with some previous researches that tested at fault resistance not more than 20 Ω and 10 Ω as in [20] and [21] respectively.

B. EFFECT OF WIND POWER

As known, incorporating wind energy systems in transmission systems results in challenges in the operation of distance protection. Such challenges are occurred because of the intermittency of the wind speed and varying the power level penetration that produce variations in both voltage and current signals during faults and the variation in source impedance inversely proportional to the wind speed and number of wind turbines. Thus, achieving proper selectivity using conventional relay is difficult with the variation of source impedance [1].

TABLE 6. The performance of the proposed distance protection scheme compared with the conventional relay for wind speed variation at different times along a day.

Actual fault conditions at 490 km				Conventional distance relay		Tripping zone of proposed scheme	
Fault type	Instant of fault (h)	Fault resistance (Ω)	Wind speed (m/s)	Relay A	Relay B	Relay A	Relay B
A-G	2:00	1	17	O	U*	CZ2	CZ1
ABC	5:00	5	14	O	U*	CZ2	CZ1
A-G	14:00	5	9.5	O	U*	CZ2	CZ1

The effectiveness of the proposed scheme to mitigate the effect of wind power is also evaluated at different wind power penetration levels. Table 5 summarizes some carried out tests for different fault types, at different locations and different fault resistance values (100 Ω for grounded faults and 20 Ω for non-grounded faults). The faults are simulated at certain wind speed (15 m/s), and different wind farm sizes (50 turbines × 1.5 MW, 100 turbines × 1.5 MW, 150 turbines × 1.5 MW and 200 turbines × 1.5 MW).As shown in Table 5, the proposed scheme has successfully detected the faults at their correct protection zones in all cases especially at the most challenging fault locations near the end boundary of zones and also the faults near buses either A or B. This correct performance irrespective to the wind penetration is achieved by applying ΔZ shifting for zones circles using the calculated Z_w, presenting the mitigation for wind farm effects described in Eqn. (11). On contrary, the conventional relay (B) at the wind farm side did not operate accurately at all cases while the conventional relay (A) has detected only some faulty cases at their true zones.

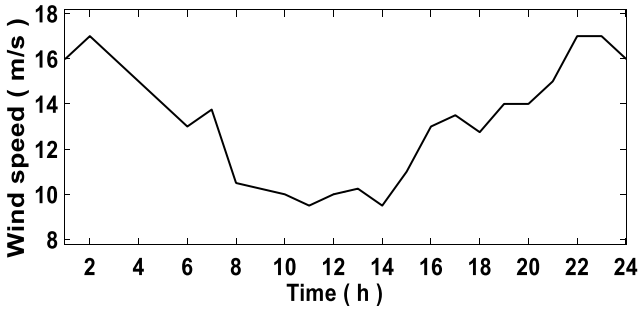

FIGURE 11. Wind speed profile during a day according to [38].

With 150 wind turbines × 1.5 MW at source B, the proposed scheme is also evaluated for wind speed fluctuations during a day according to wind speed profile in Fig. 11 [38]. In Table 6, the proposed scheme is tested for ground and non-ground faults such as A-G, ABC faults at 490 km fault location (81.67 % of the protected TL) at different times during the day, at 2:00, 5:00 and 14:00 hour, thus the wind speed are 17, 14 and 9.5 m/s respectively according to Fig.11. Comparing the fixed characteristics of the conventional relay and the updated characteristics for proposed scheme for such cases is illustrated in Fig. 12.As revealed, by the achieved adaptive shifting, the proposed scheme has avoided over-reach problems that occur in conventional distance relay A and also avoided under-reach problems that occur in conventional distance relay B.

C. EFFECT OF DIFFERENT FIRING ANGLE

In this subsection, the proposed scheme has been tested at different firing angles for capacitive mode of TCSC operation that is attained with firing angles of 65–90° [11].

By simulating different fault types, as demonstrated in Table 7, at 50 Ω for grounded faults and 20 Ω for non-grounded faults with the assumption of 15 m/s wind speed and 150 × 1.5 MW connected wind farm, the proposed scheme behavior is extensively investigated.

As shown in Table 7, the proposed scheme has operated accurately at different firing angle values compared with conventional relay. Actually, this superior behavior has also achieved even for difficult fault locations that are near to bus A and B (at 2 and 598 km) and also near to the boundary

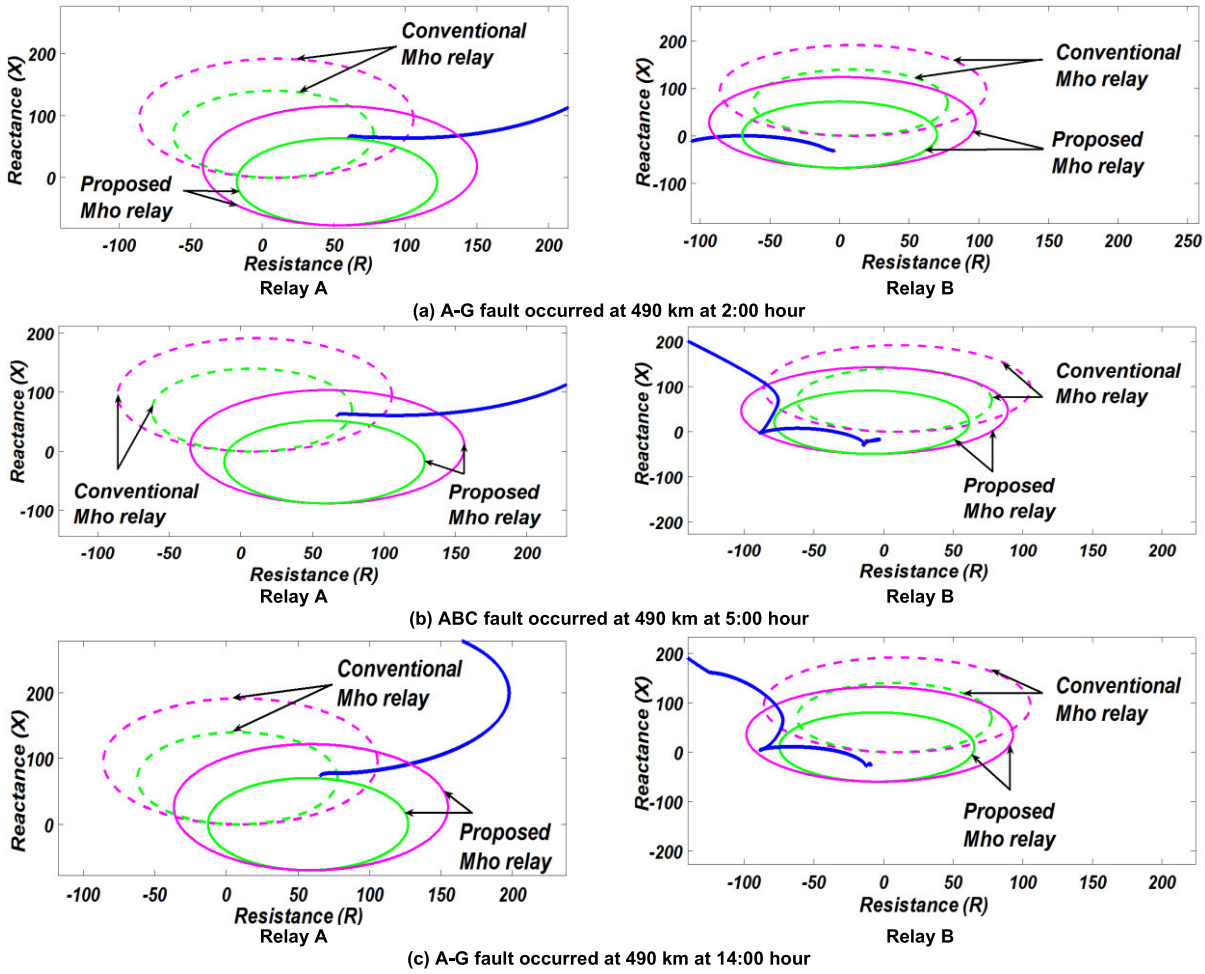

FIGURE 12. Performance of proposed Mho relay versus the conventional one during faults at 490 at different times along the day.

TABLE 7. The performance of the proposed distance protection scheme compared with the conventional relay for different firing angles of TCSC.

For SLG faults at 50 Ω fault resistance and 0° fault inception angle						For ABC faults at 20 Ω fault resistance and 0° fault inception angle					
Fault location and firing angle conditions		Conventional distance relay		Tripping zone of proposed scheme		Fault location and firing angle conditions		Conventional distance relay		Tripping zone of proposed scheme	
Fault location (km)	Firing angle (°)	Relay A	Relay B	Relay A	Relay B	Fault location (km)	Firing angle (°)	Relay A	Relay B	Relay A	Relay B
2	90	U*	U*	CZ1	CZ2	2	90	CZ1	U*	CZ1	CZ2
100	70	CZ1	U*			100	70	CZ1	U*		
200	80	U*	U*		CZ1	200	80	CZ1	U*		CZ1
301	90	U*	U*			301	90	U*	U*		
400	70	U*	U*			400	70	U*	U*		
500	80	U*	U*	CZ2		500	80	CZ2	U*	CZ2	
598	90	U*	U*			598	90	CZ2	U*		
For BC-G faults at 50 Ω fault resistance and 0° fault inception angle						For BC faults at 20 Ω fault resistance and 0° fault inception angle					
Fault location and firing angle conditions		Conventional distance relay		Tripping zone of proposed scheme		Fault location and firing angle conditions		Conventional distance relay		Tripping zone of proposed scheme	
Fault location (km)	Firing angle (°)	Relay A	Relay B	Relay A	Relay B	Fault location (km)	Firing angle (°)	Relay A	Relay B	Relay A	Relay B
2	90	CZ1	U*	CZ1	CZ2	2	90	U	U*	CZ1	CZ2
100	70	CZ1	U*			100	70	CZ1	U*		
200	80	U*	U*		CZ1	200	80	CZ1	U*		CZ1
301	90	CZ1	U*			301	90	U	U*		
400	70	CZ1	U*			400	70	CZ1	U*		
500	80	U	U*	CZ2		500	80	U	U*	CZ2	
598	90	O	U*			598	90	CZ2	U*		

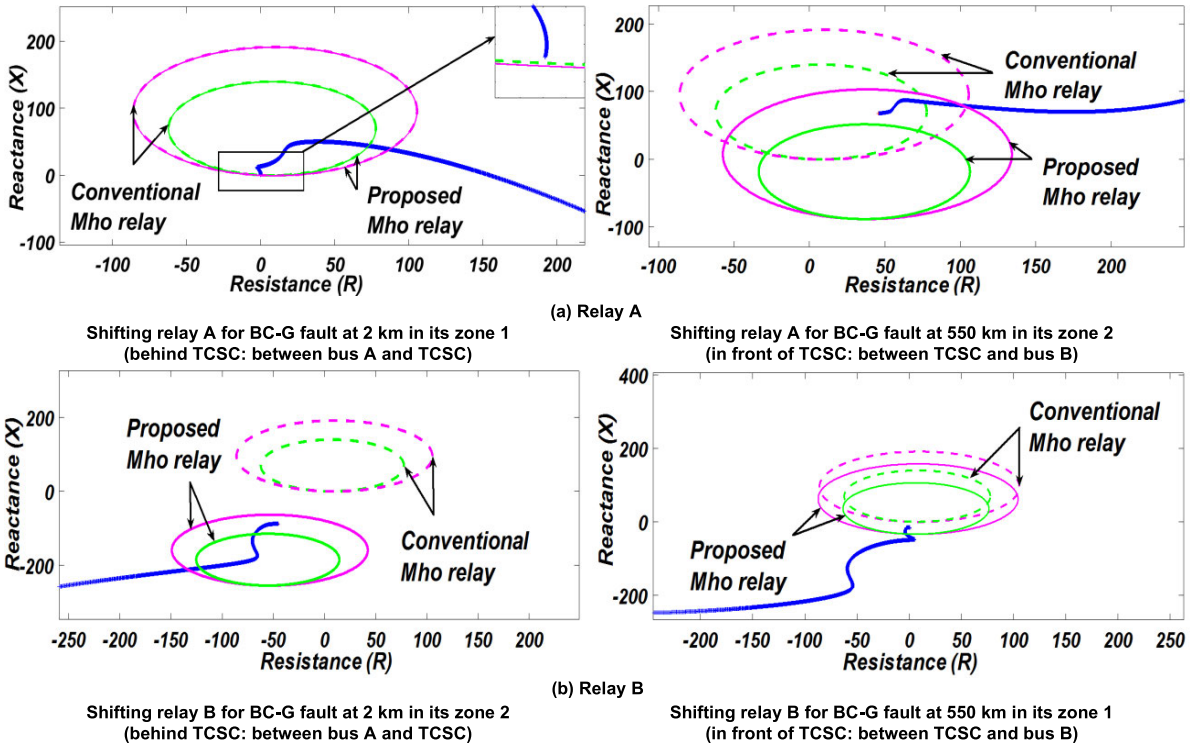

FIGURE 13. Shifting the Mho relay characteristics according to fault location w.r.t TCSC.(a) Relay A, (b) Relay B.

of the first zone for both tested relays A and B (at 100 km that presents 16.7 % of the protected TL and 500 km that presents 83.3 % of the protected TL). For all tested faulty cases, the proposed relay (either at A or B) has operated adequately and does not depend on identifying the TCSC firing angle value.

D. SHIFTING THE MHO RELAY CHARACTERISTICS ACCORDING TO FAULT LOCATION WITH RESPECT TO (W.R.T) TCSC

As discussed, the proposed scheme has improved the operation of Mho distance relay by avoiding under-reach and over-reach problems based on shifting the zones

TABLE 8. Adaptive setting of proposed distance protection for two different BC-G faults (behind / in front of TCSC).

Actual values				Estimated values				
Fault location w.r.t TCSC	Fault location (km)	Fault resistance (Ω)	Z_{TCSC} (Ω)	Fault location (km)	Fault resistance (Ω)	Z_{TCSC} (Ω)	ΔZ shifting for relay A (Ω)	ΔZ shifting for relay B (Ω)
Behind TCSC	2	200	$99.4570 \angle -96.6280^{\circ}$	3	$199.5507 \angle 0.9735^{\circ}$	$87.1120 \angle -92.4654^{\circ}$	$0.3158 \angle -96.0730^{\circ}$	$255.1610 \angle -103.8781^{\circ}$
In front of TCSC	550	0	$105.8818 \angle -89.4279^{\circ}$	543	$8.2705 \angle 84.8678^{\circ}$	$108.2099 \angle -82.5448^{\circ}$	$91.3204 \angle -68.8854^{\circ}$	$35.1792 \angle -92.1902^{\circ}$

characteristics adaptively according to different parameters. One of such parameter is the existing of TCSC in fault loop. In this section, the capabilities of the proposed scheme to accurately estimate the impedance of TCSC (Z_{TCSC}) and then to change the relay characteristics are confirmed by simulating two different faults.

- The first one is BC-G fault at 2 km (behind TCSC: between bus A and TCSC) through 200 Ω fault resistance.
- The other fault is BC-G fault at 550 km (in front of TCSC: between TCSC and bus B) through zero Ω fault resistance.

Table 8 shows the estimated values for Z_{TCSC} and R_F compared with their actual values. It also displays the characteristic shifting value (ΔZ). Then, Fig. 13 illustrates how the relay characteristics are shifted adaptively for both relay A and B to accurately detect such faults in correct zones. As illustrated, the proposed relay A has succeeded to detect the first fault (at 2 km) in its zone 1, while the second fault (at 550 km) is accurately detected in its zone 2 and vice-versa for proposed relay B.

On the other hand, the conventional Mho distance relay with fixed characteristics did not operate accurately due to the presence of wind power source; TCSC series compensator and fault resistance where under-reach and over-reach problems significantly appear. As clearly shown, the conventional distance relay A has only operated correctly for the fault at 2 km since the TCSC is not included in fault loop and the relay is very far from wind power source. As illustrated in Fig.13-a, the fixed characteristics of conventional distance relay A were very close to the characteristics of the proposed scheme due to the small required characteristic shifting value ($\Delta Z = 0.3158\Omega \angle -96.0730^{\circ}$) as depicted in Table 8.

VI. CONCLUSION

This paper has presented integrated algorithms for achieving proper distance relay operation including fault detection, classification and updating characteristics zones for relay tripping decision. To mitigate the negative effects of TCSC, wind power and fault resistance, the paper has proposed a scheme to change adaptively the settings of the Mho distance protection by shifting the relay characteristics. For implementing the proposed relay, limited communication requirements are required; as one time value is transferred in one stage, while limited RMS values, not instantaneous values, are transferred in another stage and the remaining stages are dependent on local measurements. The accurate performance of proposed scheme appears noticeably in different cases especially at challenging cases where the faults occurring near the end of the first zone and also near to buses. Finally, by getting use of technical and economic benefits of the proposed scheme, it could be used for updating, improving, and refurbishing of the existing Mho distance relays.

In the future work, the proposed scheme needs to be tested for more complex systems such as IEEE interconnected systems and also under the effects of large solar power plants.

REFERENCES

[1] K. El-Arroudi and G. Joos, "Performance of interconnection protection based on distance relaying for wind power distributed generation," *IEEE Trans. Power Del.*, vol. 33, no. 2, pp. 620–629, Apr. 2018, doi: 10.1109/TPWRD.2017.2693292.

[2] V. Telukunta, J. Pradhan, A. Agrawal, M. Singh, and S. G. Srivani, "Protection challenges under bulk penetration of renewable energy resources in power systems: A review," *CSEE J. Power Energy Syst.*, vol. 3, no. 4, pp. 365–379, Dec. 2017, doi: 10.17775/CSEEJPES.2017.00030.

[3] M. Khoddam and H. K. Karegar, "Effect of wind turbines equipped with doubly-fed induction generators on distance protection," in *Proc. Int. Conf. Adv. Power Syst. Automat. Protection*, vol. 2, Beijing, China, Oct. 2011, pp. 1349–1353, doi: 10.1109/APAP.2011.6180588.

[4] B. S. Joshi, O. P. Mahela, and S. R. Ola, "Implementation of thyristor controlled series capacitor in transmission system to improve the performance of power system network," in *Proc. 4th Int. Conf. Power, Control Embedded Syst. (ICPCES)*, Allahabad, India, Mar. 2017, pp. 1–6, doi: 10.1109/ICPCES.2017.8117644.

[5] F. B. Alhasawi, J. V. Milanovic, and A. A. Alabduljabbar, "Economic viability of application of FACTS devices for reducing generating costs," in *Proc. IEEE PES Gen. Meeting*, Minneapolis, MN, USA, Jul. 2010, pp. 1–8, doi: 10.1109/PES.2010.5590019.

[6] W. Weiguo, Y. Xianggen, Y. Jiang, D. Xianzhong, and C. Deshu, "The impact of TCSC on distance protection relay," in *Proc. Int. Conf. Power Syst. Technol. (POWERCON)*, vol. 1, Beijing, China, Aug. 1998, pp. 382–388, doi: 10.1109/ICPST.1998.728991.

[7] D. Mondal, A. Chakrabarti, and A. Sengupta, "Application of FACTS controller," in *Power System Small Signal Stability Analysis and Control*, 2nd ed. Boston, MA, USA: Academic, 2020, ch. 7, pp. 197–242.

[8] M. B. Shafik, H. Chen, G. I. Rashed, and R. A. El-Sehiemy, "Adaptive multi objective parallel seeker optimization algorithm for incorporating TCSC devices into optimal power flow framework," *IEEE Access*, vol. 7, pp. 36934–36947, 2019, doi: 10.1109/ACCESS.2019.2905266.

[9] S. Jamali and H. Shateri, "Effect of TCSC on distance relay tripping characteristic," in *Proc.39th Int. Univ. Power Eng. Conf. (UPEC)*, Bristol, U.K., Sep. 2004, pp. 704–708.

[10] S. Biswas and P. K. Nayak, "The performance evaluation of distance protection for transmission lines possessing TCSC," in *Proc. Int. Conf. Comput., Electr. Commun. Eng. (ICCECE)*, Kolkata, India, Dec. 2016, pp. 16–17, doi: 10.1109/ICCECE.2016.8009536.

[11] D. K. Ibrahim, G. M. Abo-Hamad, E. E.-D.-M. A. Zahab, and A. F. Zobaa, "Comprehensive analysis of the impact of the TCSC on distance relays in interconnected transmission networks," *IEEE Access*, vol. 8, pp. 228315–228325, 2020, doi: 10.1109/ACCESS.2020.3046532.

[12] M. Khederzadeh and T. S. Sidhu, "Impact of TCSC on the protection of transmission lines," *IEEE Trans. Power Del.*, vol. 21, no. 1, pp. 80–87, Jan. 2006, doi: 10.1109/TPWRD.2005.858798.

[13] M. A. Bhaskar and A. Indhirani, "Impact of FACTS devices on distance protection in transmission system," in *Proc. IEEE Nat. Conf. Emerg. Trends New Renew. Energy Sources Energy Manage. (NCET NRES EM)*, Chennai, India, Dec. 2014, pp. 52–58, doi: 10.1109/NCETNRESEM.2014.7088738.

[14] J. Piri, G. Bandyopadhyay, and M. Sengupta, "Effects of including SVC and TCSC in an existing power system under normal operating condition a case study," in *Proc. IEEE Int. Conf. Power Electron., Drives Energy Syst. (PEDES)*, Chennai, India, Dec. 2018, pp. 18–21, doi: 10.1109/PEDES.2018.8707541.

[15] M. Biswal, B. B. Pati, and A. K. Pradhan, "Adaptive distance relay setting for series compensated line," *Int. J. Electr. Power Energy Syst.*, vol. 52, pp. 198–206, Nov. 2013, doi: 10.1016/j.ijepes.2013.03.018.

[16] V. H. Makwana and B. R. Bhalja, "A new adaptive distance relaying scheme for mutually coupled series-compensated parallel transmission lines during intercircuit faults," *IEEE Trans. Power Del.*, vol. 26, no. 4, pp. 2726–2734, Oct. 2011, doi: 10.1109/TPWRD.2011.2159248.

[17] E. Rosolowki, J. Izykowski, A. B. Arsoy, M. M. Saha, P. Balcerek, and M. Fulczyk, "Optimization of distance protection algorithm for series-compensated transmission line," in *Proc. IEEE Trondheim PowerTech*, Trondheim, Norway, Jun. 2011, pp. 1–7, doi: 10.1109/PTC.2011.6019172.

[18] P. Mazniewski and J. Izykowski, "ATP-EMTP investigation of adaptive distance protection for transmissions lines with series compensation," in *Proc. Mod. Electr. Power Syst.*, Wroclaw, Poland, Sep. 2010, pp. 20–22.

[19] F. Wei, X. Lin, Z. Li, L. Chen, and M. S. Khalid, "A new distance protection method considering TCSC-FCL dynamic impedance characteristics," *IEEE Trans. Power Del.*, vol. 33, no. 3, pp. 1428–1437, Jun. 2018, doi: 10.1109/TPWRD.2017.2771276.

[20] A. N. Abdel-Latief, A. F. Abdel-Gawad, and M. E. Mandour, "Mitigation the effect of TCSC on the transmission lines protection devices," in *Proc. 42nd Int. Univ. Power Eng. Conf.*, Brighton, U.K., Sep. 2007, pp. 4–6, doi: 10.1109/UPEC.2007.4469009.

[21] W.-S. Seo, M.-S. Kim, S.-H. Kang, J.-S. Yoon, and C.-H. Hwang, "An improved setting method of the distance protective IEDs for series-compensated transmission lines based on a case study approach," *Electr. Power Syst. Res.*, vol. 188, Nov. 2020, Art. no. 106554, doi: 10.1016/j.epsr.2020.106554.

[22] A. Ghorbani, H. Mehrjerdi, and N. A. Al-Emadi, "Distance-differential protection of transmission lines connected to wind farms," *Int. J. Electr. Power Energy Syst.*, vol. 89, pp. 11–18, Jul. 2017, doi: 10.1016/j.ijepes.2017.01.002.

[23] S. Chen, N. Tai, C. Fan, J. Liu, and S. Hong, "Adaptive distance protection for grounded fault of lines connected with doubly-fed induction generators," *IET Gener., Transmiss. Distrib.*, vol. 11, no. 6, pp. 1513–1520, Apr. 2017, doi: 10.1049/iet-gtd.2016.1145.

[24] O. Sivov, H. Abdelsalam, and E. Makram, "Adaptive setting of distance relay for MOV-protected series compensated line considering wind power," *Electr. Power Syst. Res.*, vol. 137, pp. 142–154, Aug. 2016, doi: 10.1016/j.epsr.2016.03.048.

[25] G. Yang, M. Dong, Z. Zhou, C. Zhou, D. Du, Z. Zhan, and D. Yang, "The influences and countermeasures of wind farm access to transmission line differential protection," in *Proc. IEEE Power Electron. Mach. Wind Appl.*, Denver, CO, USA, Jul. 2012, pp. 16–18, doi: 10.1109/PEMWA.2012.6316373.

[26] M. K. Jena and S. R. Samantaray, "Data-mining-based intelligent differential relaying for transmission lines including UPFC and wind farms," *IEEE Trans. Neural Netw. Learn. Syst.*, vol. 27, no. 1, pp. 8–17, Jan. 2016, doi: 10.1109/TNNLS.2015.2404775.

[27] R. M. Mathur and R. K. Varma, *Thyristor-Based FACTS Controllers for Electrical Transmission Systems*. Hoboken, NJ, USA: Wiley, 2002.

[28] R. J. Davalos and J. M. Ramirez, "A review of a quasi-static and a dynamic TCSC model," *IEEE Power Eng. Rev.*, vol. 20, no. 11, pp. 63–65, Nov. 2000, doi: 10.1109/39.883286.

[29] D. Jovcic and G. N. Pillai, "Analytical modeling of TCSC dynamics," *IEEE Trans. Power Del.*, vol. 20, no. 2, pp. 1097–1104, Apr. 2005, doi: 10.1109/TPWRD.2004.833904.

[30] *Wind Farm—DFIG Detailed Model*. Accessed: Feb. 1, 2021. [Online]. Available: https://www.mathworks.com/help/physmod/sps/ug/wind-farm-dfig-detailed-model.html

[31] R. Gagnon, G. Sybille, S. Bernard, D. Paré, S. Casoria, and C. Larose, "Modeling and real-time simulation of a doubly-fed induction generator driven by a wind turbine," in *Proc. Int. Conf. Power Syst. Transient (IPST)*, Montreal, QC, Canada, Jun. 2005, pp. 19–23, Paper. IPST05-162.

[32] C.-H. Kim, H. Kim, Y.-H. Ko, S.-H. Byun, R. K. Aggarwal, and A. T. Johns, "A novel fault-detection technique of high-impedance arcing faults in transmission lines using the wavelet transform," *IEEE Trans. Power Del.*, vol. 17, no. 4, pp. 921–929, Oct. 2002, doi: 10.1109/TPWRD.2002.803780.

[33] M. Yumurtaci, G. Gökmen, Ç. Kocaman, S. Ergin, and O. Kiliç, "Classification of short-circuit faults in high-voltage energy transmission line using energy of instantaneous active power components-based common vector approach," *TURKISH J. Electr. Eng. Comput. Sci.*, vol. 24, no. 3, pp. 1901–1915, 2016, doi: 10.3906/elk-1312-131.

[34] A. Çapar and A. B. Arsoy, "A performance oriented impedance based fault location algorithm for series compensated transmission lines," *Int. J. Electr. Power Energy Syst.*, vol. 71, pp. 209–214, Oct. 2015, doi: 10.1016/j.ijepes.2015.02.020.

[35] Y. Hase, *Handbook of Power System Engineering*. Hoboken, NJ, USA: Wiley, 2007.

[36] L.-C. Wu, C.-W. Liu, and C.-S. Chen, "Modeling and testing of a digital distance relay using MATLAB/SIMULINK," in *Proc. 37th Annu. North Amer. Power Symp.*, Ames, IA, USA, Oct. 2005, pp. 253–259, doi: 10.1109/NAPS.2005.1560534.

[37] E. S. T. El Din, M. M. A. Aziz, D. K. Ibrahim, and M. Gilany, "Fault location scheme for combined overhead line with underground power cable," *Electr. Power Syst. Res.*, vol. 76, no. 11, pp. 928–935, Jul. 2006, doi: 10.1016/j.epsr.2005.07.008.

[38] H. Xing, H. Cheng, and L. Zhang, "Demand response based and wind farm integrated economic dispatch," *CSEE J. Power Energy Syst.*, vol. 1, no. 4, pp. 37–41, Dec. 2015, doi: 10.17775/CSEEJPES.2015.00047.

AHMED ABDEL RAHMAN MOHAMED received the B.S. degree in electrical power and machines from Helwan University, Helwan, Egypt, in 2006. He is currently pursuing the M.S. degree in digital protection in electrical engineering with Cairo University, Giza, Egypt.

Since 2007, he has been working as a designer engineer with consulting engineering companies, specialized in interior and infrastructure designs. His research interests include digital protection of power systems, utilization and generation of electric power, renewable energy sources, and alternating current transmission systems (FACTS).

HEBATALLAH MOHAMED SHARAF (Member, IEEE) received the M.Sc. and Ph.D. degrees in electrical engineering from the Department of Electrical Power and Machines, Cairo University, Egypt, in 2007 and 2015, respectively. Since 2015, she has been an Assistant Professor with Cairo University. Her current research interests include power system protection, renewable energy, power quality, and energy efficiency.

DOAA KHALIL IBRAHIM (Senior Member, IEEE) was born in Egypt, in December 1973. She received the M.Sc. and Ph.D. degrees in digital protection from Cairo University, Giza, Egypt, in 2001 and 2005, respectively.

From 1996 to 2005, she was a Demonstrator and a Research Assistant with Cairo University, where she became an Assistant Professor in 2005, an Associate Professor in 2011, and a Professor in December 2016. From 2005 to 2008, she contributed to a World Bank project in higher education development in Egypt. From January 2010 to June 2013, she contributed as an expert to the Program of Continuous Improvement and Qualifying for Accreditation in Higher Education, Egypt. From July 2013 to November 2014, she contributed as an expert to the Technical Office, Project Management Unit (PMU), Ministry of Higher Education, Egypt. Her research interests include digital protection of power systems, utilization and generation of electric power, distributed generation, and renewable energy sources.